13th International Symposium on Particle Image Velocimetry – ISPIV 2019
Munich, Germany, July 22-24, 2019

3D-reconstruction of O_2 bubble wake concentration fields

A. von Kameke[1*], F. Kexel[1], S. Rüttinger[1], R. Colombi[1], S. Kastens[1], M. Schlüter[1]

[1] University of Technology Hamburg,
Institute of Multiphase Flows,
Eissendorfer Strasse 38, 21073 Hamburg * alexandra.vonkameke@tuhh.de

Abstract

We study the concentration wake of single oxygen bubbles and pairs of bubbles rising freely in nitrogen saturated fluorophore solution using a scanning laser technique. A novel rotating polygon mirror with 36 facets and a high speed laser are synchronized as such that the consecutive light sheets can be adjusted to lie arbitrarily close together and even intersect. The measuring cell is equipped with a hypodermic needle of an outer diameter of 0.5 mm attached to a bubble generator which allows for the repeated generation of a new bubble (or bubble pair) with variable repetition rate Ohl (2001); Timmermann (2018). The usage of a hypodermic needle tip assures highly reproducible bubble rise trajectories and sizes similar to the work of Huang and Saito (2017). The data is background corrected and calibrated using an oxygen sensor attached to the inside of the measuring cell (PreSens). With this technique the three dimensional oxygen concentration in the bubble wake of a series of rising bubbles can be analyzed. We observe entangled vortical structures right before the second inflection section where the deceleration of the bubble is maximal. The highest levels of oxygen concentration occur in the interior of the vortices an reach values of up to 6 mg/L. The vortical structures are obviously entrained to rise along with the bubble.

1 Introduction

Bubbly flows play a crucial role in industry and nature. To date, the complex processes dominating mass transfer of the gas from single bubbles to the liquid phase are still being discovered. To gain a deeper knowledge of local mass transfer phenomena in bubbly flows the planar laser induced fluorescence (p-LIF) technique Bork et al. (2000, 2005); Dani et al. (2007); Kück et al. (2012); Jimenez et al. (2013); Timmermann et al. (2016); Huang and Saito (2017) was successfully used in different experimental arrangements. Small bubbles with diameters of ≈ 1 mm which rise on a straight path and have a rotationally symmetric wake have recently been investigated by Laser Induced Fluorescence (LIF) measurements and numerical simulations Weiner et al. (2019). The mass transfer of an elliptic, wobbling bubble which prescribes a complex three-dimensional rising path cannot be addressed by these measurements in one single plane. Therefore during the last years a measurement technique called time resolved scanning laser induced fluorescence (TRS-LIF) was developed Timmermann (2018); Brücker (1999); Deusch and Dracos (2001); Crimaldi (2008); Stöhr et al. (2009); Soodt et al. (2012); Huang and Saito (2017). Here, for this measurements the technique is adapted in two ways: Firstly, the oxygen measurement for the calibration reference images was placed directly in the measurement cell allowing for an online integral oxygen concentration measurement. Secondly, the rotating mirror was replaced by a mirror with more facets (36 instead of formerly 21).

2 Experiments

The basic setup, shown in Fig. 1, is an adapted version of the set-up introduced by Timmermann et al. (2016); Timmermann (2018); Weiner et al. (2019). The bubbles rise in a square measuring cell with a cross section of $150x150\,\mathrm{mm}^2$. The side walls are made of glass, while the bottom and the lit are made of stainless steel with customized openings that allow for different experimental arrangements. An opening at the lit

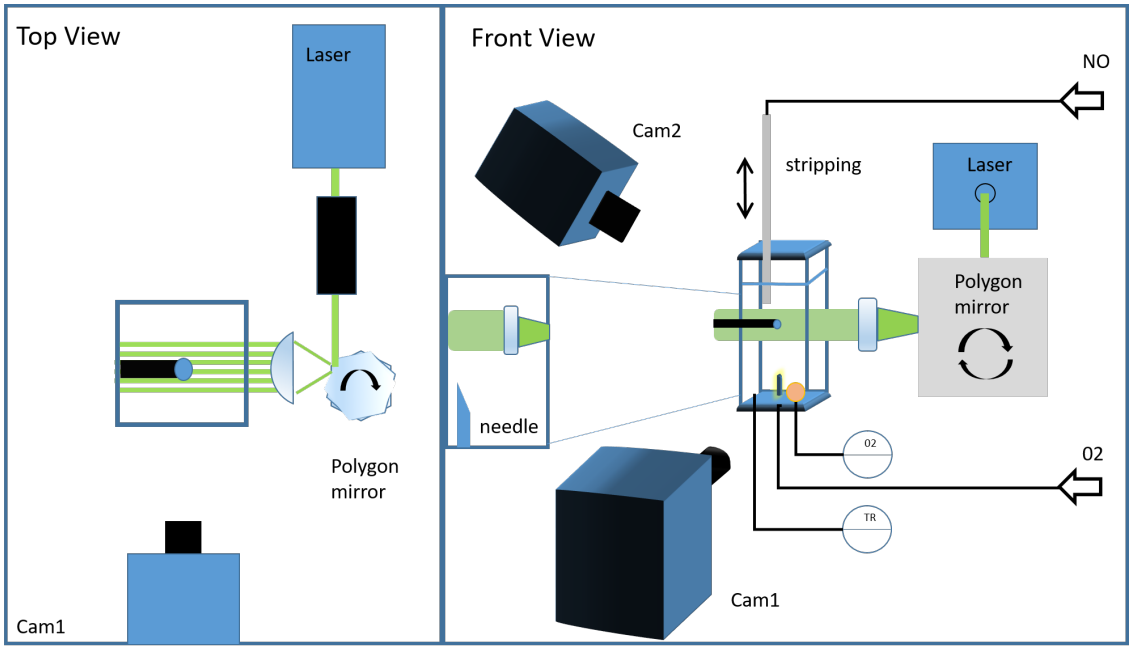

Figure 1: The experimental set-up comprises two high-speed cameras. One is recording the quenched fluorescence in the bubble wake (cam1), while the second camera (cam2) allows to observe the resulting light sheets and its characteristics (thickness, inter light sheet distance, temporal evolution).

at the top allows the insertion of a sparger that can be used for stripping of the experimental solution with a desired gas. Throughout these experiments nitrogen (N_2, 99.95 vol%, Westfalen AG) was used for stripping for around 20 min prior to the experimental run, assuring thus an oxygen free solution. The oxygen concentration is monitored during the whole measurement with a PreSens oxygen sensor probe within the measuring cell.

An oxygen bubble is generated according to Timmermann (2018) in the center of the bottom where a hypodermic needle can be fixed using an inserted screw thread. In this way the opening of the needle can be turned into any desired direction, allowing for the adaption of the view of the camera with respect to the bubble trajectory. Here, a hypodermic needle of outer diameter 0.5 mm was positioned with the needle tip opposite to the laser sheet (see inset Fig. 1). The usage of a hypodermic needle allows for a high reproducibility of the bubble path Huang and Saito (2017). The size of the bubble depends on the flow rate passing through the needle and needs to be adjusted very well. We control the flow rate regarding to Ohl (2001), where the bubble volume is altered by an injection valve that is controlled via a function generator. In this way the duration of the opening as well as the repetition rate of bubbles can be adjusted and, together with the needle opening, the flow rate is fixed. For the experiments shown the resulting oxygen bubble had an elliptic shape and an equivalent diameter of $2.6-2.9$ mm resulting in a typical helical rising path. The bubbles sizes are thus considerably smaller than previously reported Timmermann (2018).

In order to measure the dissolved oxygen in the wake of the bubble, time resolved scanning laser induced fluorescence (TRS-LIF) is used (ILA_5150 GmbH). A schematic top view of the setup for TRS-LIF, based on the work of Soodt et al. (2012) is shown in Fig. 1. The laser sheet is reflected from a rotating polygon (36 faces) into the measurement volume. The laser used is an Nd:YLF laser (Quantronix: Darwin$Duo 527-100-M now Continuum®: TerraTM PIV; wavelength 527 nm). The synchronization of the polygon rotation and the laser pulse emission can be adjusted in order to vary the number of light sheets, the volume scan rate and the inter light sheet distance. The rotational speed of the polygon is limited to 10000 rpm $\approx$ 166.6667 Hz while the maximum pulse rate of the laser is 20000 Hz. Here, the polygon rotation was set to its maximum. An additional laser and a photodiode detect the actual rotation speed of the polygon mirror and act as the master trigger for the laser and the cameras assuring that after each volume scan all signals are synchronized. The single light sheets were adjusted to an approximate minimal thickness of 0.5 mm,. With $N = 40$ light sheets and a laser pulse rate of 6400 Hz light sheets to lie arbitrarily close

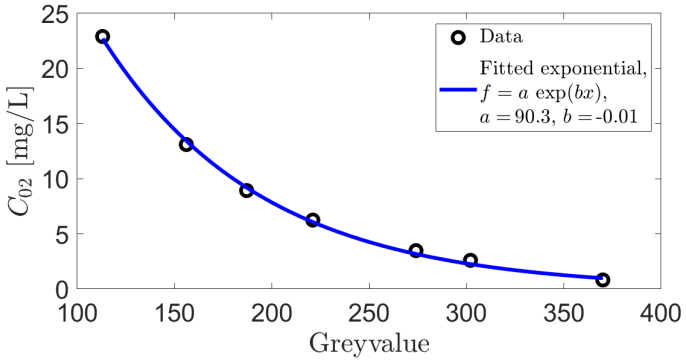

Figure 2: An exponential calibration function was fitted to each pixel of each light-sheet seperately. An exemplary fit for image pixel 600, 500 of slice 30 is shown. For each concentration value six volume scans have been averaged.

together as was measured by a second camera (cam2). Both cameras (pco.dimax HS2, equipped with a Carl Zeiss 50mm Makro-Planar) were set to the same recording frequency as the laser and triggered via the same signal, taking advantage of the fact that frame rate can be increased when resolution is decreased.

To obtain quantitative measurements of the dissolved oxygen in the bubble wake a fluorophore Dichlorotris (1, 10-phenanthroline) ruthenium(II) hydrate ($c = 30\,\mathrm{mg/L}$; Sigma-Aldrich) is used Timmermann et al. (2016). The fluorescence of this dye shows a dependence of the oxygen concentration due to quenching which can be described with a Stern-Volmer correlation Kück et al. (2012). The emitted fluorescence light excited with the laser light sheets is recorded with the camera, protected by a bandpass filter (ILA_ 5150 GmbH, center wave length $590\,\mathrm{nm} \pm 2\,\mathrm{nm}$, half-power bandwidth nm2nm , transmission $> 84\%$) from direct laser radiation, perpendicular to the laser sheet, see Fig. 1.

Intensity calibration measurements were performed directly in the measurement cell at seven different oxygen concentrations ranging from $0 - 23\,\mathrm{ppm}$. The procedure was as follows: After the experimental run was performed the set-up was flushed alternately with oxygen and nitrogen in order to obtain a well mixed state with a stable oxygen level. This level was constantly monitored and measured using the PreSens oxygen sensor. Only after reaching a constant level and by assuring visually that no concentration gradients were left in the solution the calibration measurements were recorded going through the same measurement protocol used during the recording of the bubble wake. In this way, six volume scans with 40 light sheets were recorded for each oxygen concentration.

3 Results

3.1 Image analysis

In order to be able to associate a grey value to an oxygen concentration an exponential fit to the measured data was performed for each image pixel of every light sheet (40 light sheets in one volume scan). An example is shown in Fig.2. To reduce noise in the calibration images each of the light sheets was averaged over six volume scans at each oxygen level. In this way two calibration matrices A and B were derived for each light sheet.

The corresponding calibration matrices A, B were then used to convert the gray scale values in each image to oxygen concentration values in units of $\mathrm{mg/L}$. However, the TRS-LIF images are additionally altered by a stripy pattern. Most likely this pattern occurs because of attenuated laser intensity due to hardly avoidable dust on the rotating mirror. Since the mirror speed is fluctuating slightly the laser does not visit the very same spot periodically and the resulting stripy pattern does never repeat exactly. These stripes bias the concentration values and are hindering to the reconstruction of the bubble wake. Therefore, in order to reduce the effects of the stripes we take advantage of our knowledge about the boundary conditions of the experiments. Since we know that right after stripping there is still zero oxygen level on both sides

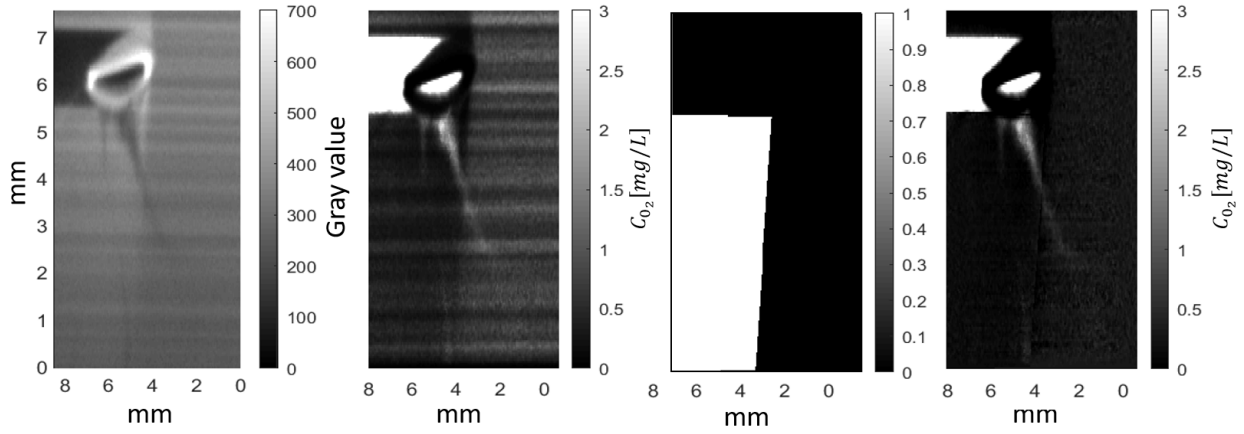

Figure 3: The figure shows from left to right: (1) The raw recorded image (slice 29), where high concentrations of oxygen are seen as dark areas in the bubble wake; (2) the calibrated image, where each pixel was converted using the calibration coefficients from an exponential fit; (3) a binary mask that is created manually via a customized algorithm; (4) the final image used for the wake analysis where the stripy pattern has been removed via the subtraction of a reference profile either from the left (mask = 1) or from the right side of the bubble (mask = 0). This distinction becomes neccessary due to the reflection of the bubble when the light sheet hits it.

of the bubble trajectory we can take a vertical reference profile from the left or right edge and subtract it everywhere in the picture. The procedure is depicted in Fig. 3. However, the stripes are not perpendicular to the image boundaries and the image needs to be rotated before subtracting the reference profile. This procedure works well as long as the light sheet does not hit the bubble. In this case, the bubble reflects the light sheet under a certain angle and makes some regions brighter than others. In these cases (around 5-7 images in one volume scan) a customized algorithm allows for a manual definition of the brighter region which is then subtracted by the reference profile from the side closer to the region (in Fig. 3 it corresponds to the left side).

3.2 Rising paths, wake structures and O_2 concentration field

Fig. 4 shows the rising paths of four consecutively rising bubbles (different symbols). The experiments shown here focus on the second inflection section right after the first inflection point similar as in Huang and Saito (2017) since we expected maximal deceleration and therefore interesting wake structures. Due to the creation of the bubbles using a hypodermic needle as described above the rising paths of the bubbles are largely reproducible. However, they do deviate more then reported in literature Huang and Saito (2017). Preliminary results from time resolved scanning particle image velocimetry (TRS-PIV) suggest, that the bubble repetition rate of 1,Hz was still too fast and that the liquid has not fully settled to zero velocity in between two consecutive bubbles. The repetition rate should thus be chosen smaller in follow-up studies but it must be taken into account that one cannot get arbitrarily slow because other unwanted effects such as diffusion of nitrogen gas from the oversaturated solution into the needle might occur resulting in bubbles of gas mixtures. An effect on oxygen concentration was observed qualitatively since after nitrogen stripping the first two bubbles oftentimes showed only a very faint wake.

After the elaborate image processing the wake structure can be reconstructed three-dimensionally as shown in Fig. 5. Here the voxels have a size of $(0.042 \times 0.042 \times 0.5)\,\mathrm{mm}^3$. Two typical horseshoe like structures are distinguishable, similar to those described by Huang et al. Huang and Saito (2017) for a mean wake of several CO_2 bubbles rising in clean and contaminated water. However, in this study no binarization of the concentration fields was used to obtain the wakes but a direct calibration and some image correction as elaborated above. Further, for the first time, these structures and their concentration distributions are quantitatively analyzed from single bubbles. The spatial resolution is thereby around five times coarser then in claimed in Huang and Saito (2017) and is limited by our light sheet thickness. It is thus very likely that we miss fine structures of less than a voxel size which do exist in the vicinity of the second inflection section.

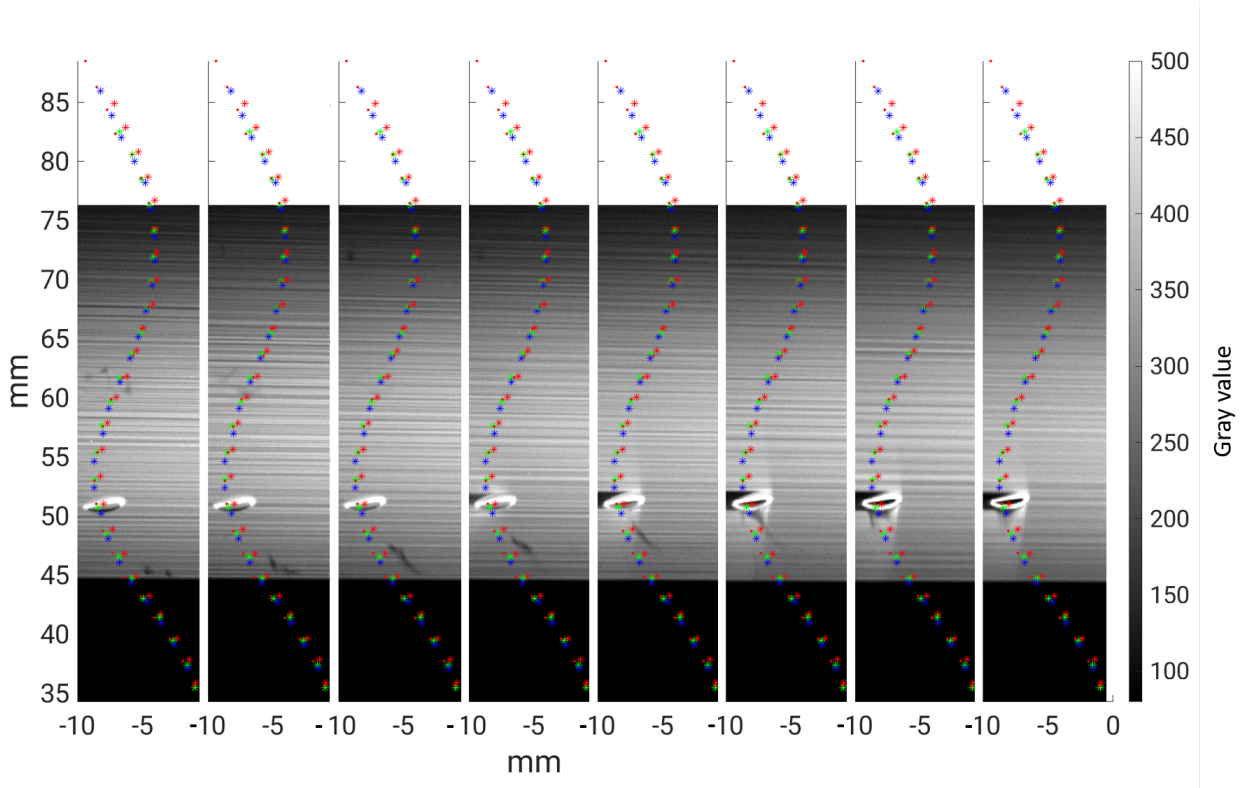

Figure 4: Four bubble rising path have been analyzed and the center of mass of each is plotted in time on its rise (different colored symbols). In the background an image sequence of the first volume scan is depicted, showing the raw-images of a bubble and its concentration wake.

The two typical horseshoe like structures further rise upwards with the bubble, since they are entrained by the bubbles rise. It can be clearly seen, that the oxygen concentration is highest inside the vortex cores and that it decrease only slightly with time. This finding suggests that the vortices have a stabilizing effect and might locally prevent the dissolved oxygen from mixing with the surrounding fluid.

4 Conclusion

We have shown that it is feasible to reconstruct the bubble wake of a freely rising elliptical bubble undergoing shape oscillations via TRS-LIF. To achieve an acceptable image quality we used the existence of side areas of the image where the oxygen concentration is still zero. To our knowledge, the concentration wake of a single rising elliptical bubble has not been analyzed quantitatively before. The preliminary results exhibits structures similar to those reported literature. Further analysis, e.g. of the amount of total transferred oxygen concentration in the wake in time remains to be calculated. Also, further bubbles need to be analyzed in order to be able to compare the fluctuations. The results further suggest that spots of high oxygen concentration form that stay ”coherent” during a considerable amount of time (seconds) and prevent the dissolved oxygen from mixing. This could potentially affect organisms and chemical reactions that depend on the concentration of the dissolved gas.

Acknowledgements

We thank the German Research Foundation (DFG) for the funding this research within the priority program “Reactive bubbly flows” SPP 1740 (SCHL 617/12-2). We thank Ms. Claire Claasen and Dr. Maike Baltussen for fruitful discussion.

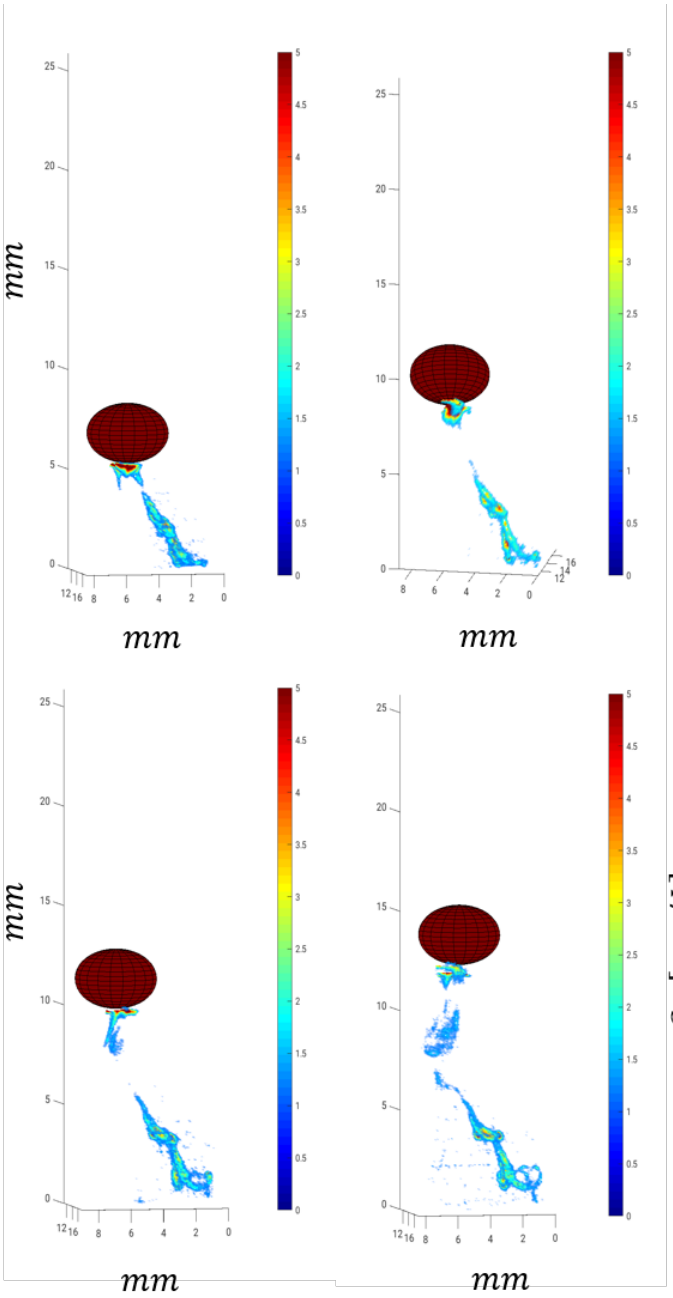

Figure 5: The concentration wake has been reconstructed putting all slices together and assuming the resolution in the scanning direction to be 0.5 mm (light sheet thickness). Two typical horseshoe like structures can be distinguished that further rise upwards since they are entrained by the bubbles rise. It can be clearly seen, that the oxygen concentration is highest inside the vortex cores and that is almost does not decrease during the successive time steps. The ellipsoid indicates the location of the rising bubble qualitatively.

References

Bork O, Schlüter M, and Räbiger N (2000) Untersuchungen zum lokalen stoffaustausch an frei aufsteigenden blasen durch visualisierung des sauerstoffkonzentrationsfeldes mit hilfe der laserinduzierten fluoreszenzmesstechnik. in D et al, editor, *Lasermethoden in der Strömungsmesstechnik*. pages 32.1–32.7. Shaker Verlag, Aachen

Bork O, Schlüter M, and Räbiger N (2005) The impact of local phenomena on mass transfer in gas-liquid systems. *Can J Chem Eng* 83:685–666

Brücker C (1999) Structure and dynamics of the wake of bubbles and its relevance for bubble interaction. *Physics of fluids* 11:1781–1796

Crimaldi J (2008) Planar laser induced fluorescence in aqueous flows. *Experiments in fluids* 44:851–863

Dani A, Guiraud P, and Cockx A (2007) Local measurement of oxygen transfer around a single bubble by planar laser-induced fluorescence. *Chemical Engineering Science* 62:7245–7252

Deusch S and Dracos T (2001) Time resolved 3d passive scalar concentration-field imaging by laser induced fluorescence (lif) in moving liquids. *Measurement Science and Technology* 12:188

Huang J and Saito T (2017) Influences of gas–liquid interface contamination on bubble motions, bubble wakes, and instantaneous mass transfer. *Chemical Engineering Science* 157:182–199

Jimenez M, Dietrich N, and Hébrard G (2013) Mass transfer in the wake of non-spherical air bubbles quantified by quenching of fluorescence. *Chemical Engineering Science* 100:160–171

Kück UD, Schlüter M, and Räbiger N (2012) Local measurement of mass transfer rate of a single bubble with and without a chemical reaction. *J Chem Eng Jpn* 45:708–712

Ohl CD (2001) Generator for single bubbles of controllable size. *Review of Scientific Instruments* 72:252–254

Soodt T, Schröder F, Klaas M, van Overbrüggen T, and Schröder W (2012) Experimental investigation of the transitional bronchial velocity distribution using stereo scanning piv. *Experiments in fluids* 52:709–718

Stöhr M, Schanze J, and Khalili A (2009) Visualization of gas–liquid mass transfer and wake structure of rising bubbles using ph-sensitive plif. *Experiments in fluids* 47:135–143

Timmermann J (2018) *Experimental analysis of fast reactions in gas-liquid flows*. Cuvillier Verlag Göttingen, Band 3, 130 Seiten

Timmermann J, Hoffmann M, and Schlüter M (2016) Influence of bubble bouncing on mass transfer and chemical reaction. *Chem Eng Tech*

Weiner A, Timmermann J, Pesci C, Grewe J, Hoffmann M, Schlüter M, and Bothe D (2019) Experimental and numerical investigation of reactive species transport around a small rising bubble. *Chemical Engineering Science: X* 1:100007